Am J Blood Res 2021;11(1):84-92
www.AJBlood.us /ISSN:2160-1992/AJBR0129596

Original Article

A novel ultrasound-based approach to investigate extramedullary haematopoiesis in foetal spleen

Marcello Roberto[1*], Gianmario Pasqualone[1*], Nicola G Di Donato[2], Zaheer Malik[6], Sheereen Bhaiyat[6], Vito CA Caponio[4], Giuseppe Lillo[5], Gianfranco Vallone[1], Ciro R Rinaldi[3,6], Vincenzo Martinelli[1]

[1]Department of Medicine and Health Sciences "Vincenzo Tiberio", University of Molise, Campobasso, Italy; [2]Obstetrics and Gynaecology Operating Unit, "Antonio Cardarelli" Hospital, Azienda Sanitaria Regionale del Molise (ASReM), Campobasso, Italy; [3]Joseph Banks Laboratories, School of Life Sciences, College of Science, University of Lincoln, Lincoln, United Kingdom; [4]Department of Clinical and Experimental Medicine, University of Foggia, Foggia, Italy; [5]Master's Degree in Computer Engineering at Polytechnic University of Turin, Torino, Italy; [6]Haematology Department, Pilgrim Hospital, United Lincolnshire Hospitals Trust (ULHT), Boston, United Kingdom. [*]Equal contributors and co-first authors.

Received January 5, 2021; Accepted February 4, 2021; Epub February 15, 2021; Published February 28, 2021

Abstract: Foetal spleen is described as a transient focus of haematopoiesis between the 3rd and 5th month of gestation: this function is however entirely replaced by the bone marrow before the end of pregnancy. This study identifies haematopoiesis in foetal spleen by exploring changes of echogenicity during its development throughout gestation. Two intervals of pregnancy were studied: Mid-Pregnancy (Mid-P, 19-23 weeks) and End-Pregnancy (End-P, 37-41 weeks). The foetal spleen was investigated in 80 pregnant women (41 vs 39). Due to quality criteria the comparison was made between 60 images (30 Mid-P vs 30 End-P). The acquisition of splenic parenchyma was followed by clustering segmentation. We identified two new parameters resulted from the clustering segmentation: Dark Ratio (DR) and Light Ratio (LR). These are related to splenic echogenicity expressing the percentage of dark and light signal in the clustered image, influenced by blood cellularity. The mean of DR value was different among the 2 groups (0.0631 vs 0.0483, $P = 0.014$), while LR did not show any significant differences. We conclude that DR may represent a reliable radiomic parameter in the determination of extramedullary haematopoiesis in the spleen.

Keywords: Foetal spleen, extramedullary haematopoiesis, ultrasound, radiomics, clustering segmentation

Introduction

Spleen is the largest lymphoid organ in human body. It appears at 5th-6th week of gestational age (GA) on the left side of the dorsal mesogastrium [1]. From the 18th week of GA, two functionally distinct compartments arise: the red and white pulp [2]. Haematopoiesis can be detected in foetal spleen from the third month of pregnancy [3-6]. This function is transitional and tends to be replaced by the bone marrow (BM) at the sixth-seventh month [7]. After delivery, spleen acquires the germinal centres which give the definitive lymphoid structure [2].

The role of foetal spleen in extramedullary haematopoiesis (EMH) is still controversial, however, many studies support its function as mid-gestation haematopoietic organ [4, 7, 8]. The assumption of haematopoietic activity in foetal spleen is historically based on murine models [2, 9]: haematopoietic development of spleen in humans parallels that of mouse [10].

Increasing evidence [6, 8, 11] reveals that haematopoietic stem cells (HSCs) can be collected from foetal spleen: the migration into the organ may occur during the first trimester of pregnancy. Electron microscopy studies [12] confirm presence of resident splenic immature HSCs at the first and second trimester, possibly as result of their entrapment from foetal blood, rich of HSCs [13, 14]. However, this finding seems to be a transient phenomenon: HSCs are not observed in spleen at the ninth month [11], when the blood still contains an amount of CD34+ three times that of adult BM [5, 15].

An increase of absolute number of CD34+ cells in human foetal spleen is detectable: 1×10^6 at

16-17 weeks of GA to 11×10^6 at 21-22 weeks of GA; notably the spleen exhibits the higher percentage increase of CD34+ compared to BM and foetal liver [16].

In adult life, spleen may reacquire its role in EMH under certain circumstances, such as infections, inflammations and malignancy [17]. A typical example is what happens in the setting of myelofibrosis, a disease in which BM becomes inhabitable [18]. The haematopoietic stem and progenitor cells migrate and seed in the spleen: these cells initiate splenic EMH. However, this new microenvironment is not suitable as the BM, therefore this EMH is ineffective [19].

Spleen may be investigated through ultrasound (US) only from the 18th week of GA [20]. Previous studies [20, 21] generated US splenic nomograms to characterize the growth of foetal spleen during pregnancy. However, the sonographic appearance of parenchyma was not considered.

US represents the technique of choice for regular monitoring of pregnancy [22]; the extension of radiomic analysis may constitute a promising approach in this field [23-25]. The spread of this novel technique is transforming the conception of diagnosis and prognosis in medical imaging [23]. However, there are no published data on the use of radiomic analysis investigating the spleen by using US, but only on computed tomography technique [24].

The aim of this work is to assess the echogenicity of foetal spleen during pregnancy by using US imaging, in order to identify splenic EMH. Our study constitutes the first assessment of splenic echogenicity through two radiomic parameters, which resulted from clustering segmentation of the images [25, 26].

To evaluate any significant differences, two groups were studied: Mid-Pregnancy (Mid-P, 19-23 weeks of GA) and End-Pregnancy (End-P, 37-41 weeks of GA).

Material and methods

Patient population

The study was conducted at "Antonio Cardarelli" hospital in Campobasso, Molise, Italy. A total number of 80 (41 Mid-P vs 39 End-P) different healthy pregnant women were retrospectively enrolled in this study. They had given their written consent to collect and publish the US images of foetal spleen and their own information, anonymously. Due to the spread of COVID-19 pandemic, our group of study decided to stop further recruitment because of a slower-than-anticipated enrolment rate, that rendered the number of participants unlikely to reach the projected target within a reasonable time frame. Data related to hypertension, dyslipidaemia, diabetes, smoking history, alcohol, drug use, age, weight, height and ethnicity group were collected. Patients characteristics are summarized in **Table 1**. This work received the approval by the "Comitato Etico Università Federico II" ethics committee of University of Naples Federico II (n. 400/20).

Ultrasound examination

The US scans were performed using the 2D Esaote MyLab™ Seven eHD Crystaline, AC2541 1-8 MHz convex US probe, on "obstetrics" machine setting. All the scans were acquired by the same operator, who was blind to the study. After each US examination, the acquired scans were stored in the digital diagnostic imaging archive of Obstetrics and Gynaecology Operating Unit. GA was estimated by US foetal biometry [20]. The spleen was best selected and visualized on axial abdominal scan, in absence of acoustic shadows involving the organ, when the foetus lied in an occipito-posterior position [27]: gastric bubble and first portion of umbilical vein were chosen as reference points to select comparable scans (**Figure 1**). The dimensional parameters (*length*, *width*, *circumference* and *area*) were digitally measured and registered as the average of three different measurement: resulting values were aligned with splenic nomograms of previous studies [20, 21]. Presence of maternal (gestational diabetes, pre-eclampsia, infections), foetal (small for gestational age, large for gestational age), placental (placenta previa, accreta, abruptio placentae) and/or amniotic (oligo- or polyhydramnios) pathological conditions and/or multiple gestations were defined as exclusion criteria. Only two pregnant women in the End-P group were under anti-hypertensive agents. Inclusion criteria are described as follows: in Mid-P group were included healthy foetuses at

Table 1. Features of the pregnant women *(Mean ± SD)*

		n	*GA (weeks)*	*Age (years)*	*Weight (kg)*	*Height (m)*	*BMI*	*Hypertension*		*Diabetes*		*Dyslipidaemia*		*Smoke*		*Ethnicity*	
								no	*yes*	*no*	*yes*	*no*	*yes*	*no*	*yes*	*white*	*black*
Group	*Mid-P*	41	20.39 ± .74	29.78 ± 6.00	65.09 ± 8.81	1.64 ± .06	24.16 ± 2.48	41	0	41	0	39	2	31	10	36	5
	End-P	39	38.62 ± 1.44	34.18 ± 4.96	77.97 ± 14.00	1.66 ± .06	28.10 ± 4.51	36	3	38	1	37	2	35	4	36	3

Abbreviations: Mid-P (Mid-Pregnancy), End-P (End-Pregnancy), n (number), GA (Gestational Age), BMI (Body Mass Index), SD (Standard Deviation).

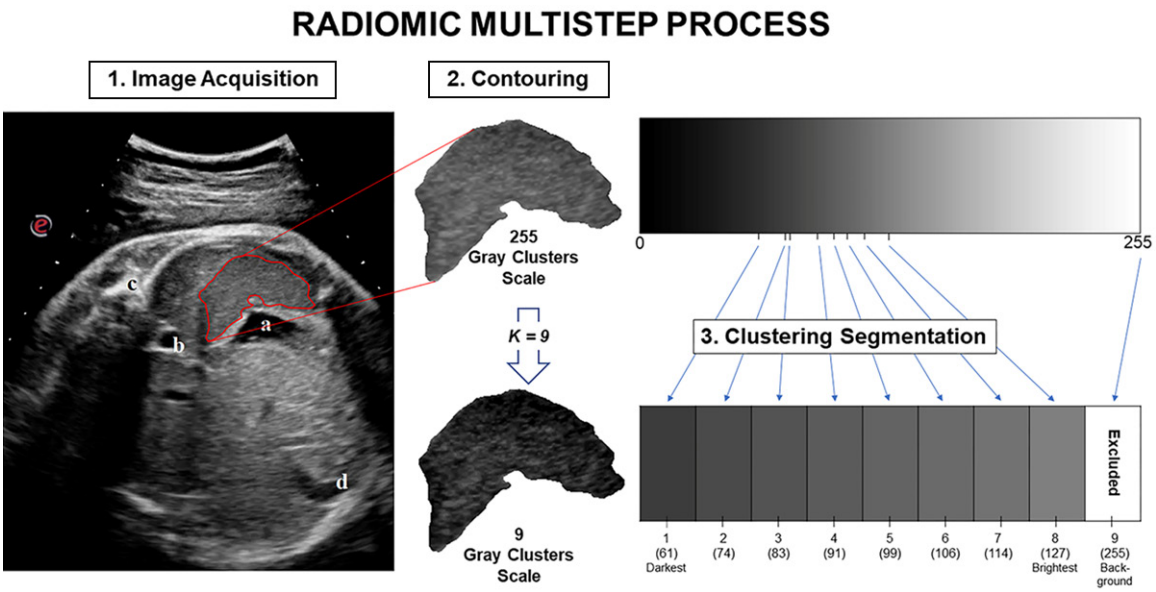

Figure 1. Schematic representation of radiomic workflow (k = 9 in k-means algorithm). 1. Detection of foetal spleen in the abdominal scan (red trace): a - gastric bubble, b - aorta, c - vertebra, d - umbilical vein. 2. Computed isolation of spleen parenchyma ("region of interest") from adjacent structures. 3. Image conversion from a 0-255 to 1-9 greyscale clusters. As neutral background of clustered image, white cluster is not considered the brightest cluster.

19-23 weeks of GA; in End-P group were included healthy foetuses at 37-41 weeks of GA. Spleen images were considered for inclusion only if abdominal scans (axial view), with a clearly visible spleen, without acoustic shadows involving the region of interest and in presence of the aforementioned reference points.

From February 2019 to February 2020, a total of 80 images were collected (41 vs 39). Twenty images were excluded (13 malposition, 2 small for gestational age, 1 gestational diabetes, 2 pre-eclampsia, 2 oligohydramnios). The remaining 60 images, 30 Mid-P and 30 End-P were analysed, thus underwent clustering segmentation. We digitally isolated the splenic parenchyma by photo editing software (Adobe Photoshop® CC 2017): this tool allowed the accurate isolation of spleen parenchyma, preserving images and informative content quality (**Figure 1**).

Computer processing

Radiomics is a new challenging approach that transforms digitally encoded medical images into mineable high-dimensional data [28]. The first step consists of image acquisition, followed by the segmentation of the "region-of-interest" [25]. In this study the algorithm k-means was used as part of clustering segmentation [26]. The K-Means algorithm operates finding and grouping datapoints in classes that have high similarity between them. This similarity is understood by the system as the opposite of the distance between datapoints. The closer the data points are, the more similar and more likely to belong to the same cluster (see below) they will be [25]. The distance between the datapoints is calculated by Euclidean distance.

The algorithm works through several steps: a) selection of the "k" number of clusters in which the datapoints need to be grouped; b) first random selection of the cluster centroids; c) assignment of each datapoint to the closest centroid; d) calculation of within-the-cluster-sum-of-squares value; e) final definition of the "new" centroids by calculation of the minimum quadratic error between datapoints and the centre of each cluster; f) re-assignment of the datapoints to the definitive centroids. This process can be repeated multiple times.

In this study, the datapoints represent the pixels within the grayscale image (single channel grayscale map) of the isolated spleen parenchyma (the "region of interest"): every pixel in the image is defined by one grayscale value, so similarities can be detected from the system.

Here the k-means assigns each pixel of the greyscale scan (0 to 255 shades of grey; 0 -

Table 2. Differences in foetal splenic parameters of Mid-P and End-P groups. DR9 and LR9 values are shown *(Mean ± SD)*

		Length (mm)	*Width (mm)*	*Circumference (mm)*	*Area (mm^2)*	*DR9*	*LR9*
Group	*Mid-P*	14.99 ± 2.50	8.28 ± 1.41	42.42 ± 5.65	.95 ± 0.23	.063 ± .026	.039 ± .025
	End-P	40.42 ± 6.31	16.79 ± 3.21	113.12 ± 17.12	5.68 ± 1.67	.048 ± .018	.036 ± .020

Abbreviations: Mid-P (Mid-Pregnancy), End-P (End-Pregnancy), DR9 (Dark Ratio, when k = 9 in k-means algorithm), LR9 (Light Ratio, when k = 9 in k-means algorithm), SD (Standard Deviation).

Table 3. Pearson rank correlation analysis

Variable	*GA*	*Weight*	*Height*	*BMI*	*DR9*	*LR9*
GA	P = 1	0.504	0.219	0.495	-0.298	-0.065
	p-value = 1	< 0.001	0.051	< 0.001	0.021	0.619
Weight		P = 1	0.572	0.928	-0.172	-0.083
		p-value = 1	< 0.001	< 0.001	0.188	0.528
Height			P = 1	0.229	-0.023	0.081
			p-value = 1	0.041	0.862	0.539
BMI				P = 1	-0.181	-0.125
				p-value = 1	0.166	0.341
DR9					P = 1	-1.48
					p-value = 1	0.258
LR9						P = 1
						p-value = 1

Abbreviations: GA (Gestational Age), BMI (Body Mass Index), DR9 (Dark Ratio, when k = 9 in k-means algorithm), LR9 (Light Ratio, when k = 9 in k-means algorithm).

black, 255 - white) into a "k" number of clusters. Furthermore, the algorithm calculates the absolute number of pixels within the clusters with the darkest (Dark Cluster-*DC*) and brightest (Light Cluster-*LC*) centroids. Also, the system calculates the percentage of pixels attributed to the DC and to the LC in relation to the total number of pixels in the region of interest: Dark Ratio (DR) and Light Ratio (LR), respectively. After the k-means algorithm run, the isolated region of interest is clustered in a "k-1" number of clusters: one cluster is always excluded because it constitutes the white background surrounding the image. **Figure 1** shows a visual representation of the segmentation algorithm, run with k = 9: each pixel of the image is assigned to one of the 8 clusters, and is represented using the greyscale colour that corresponds to the value of the centroid assigned to its own cluster.

K-means algorithm was run with a convergence tolerance value of 0.0001, using the k-means++ cluster initialization method [29] and each run was executed 4 times, selecting the best one on the basis of the within-the-cluster-sum-of-square score. The clustering segmentation was carried out in six different number of clusters (k = 4, 5, 6, 7, 8, 9); values of *DR* and *LR* for each clustering were calculated (*DR4-LR4, DR5-LR5, DR6-LR6, DR7-LR7, DR8-LR8, DR9-LR9*). The "silhouette score" [26] was determined as a cluster validity method for each number of clusters: k = 9 exhibited the higher value (0.7774). Therefore, *DR9* and *LR9* were used to match the two groups. Splenic parameters are summarized in **Table 2**.

Statistical analysis

Shapiro-Wilk test was used to investigate the normal distribution of *DR9* and *LR9* parameters [30]. Because of the normal distribution of variables, parametric tests were used. Pearson rank correlation analysis was performed to investigate the relation between *DR9* and *LR9* with the weeks of gestations, weight, height and body mass index of pregnant women. The difference in *DR9* and *LR9* between the groups was further investigated through the independent samples t-test and ANOVA one-way test. Since *DR9* showed a normal distribution in Mid-P group and non-normal in End-P group, we performed both the independent samples

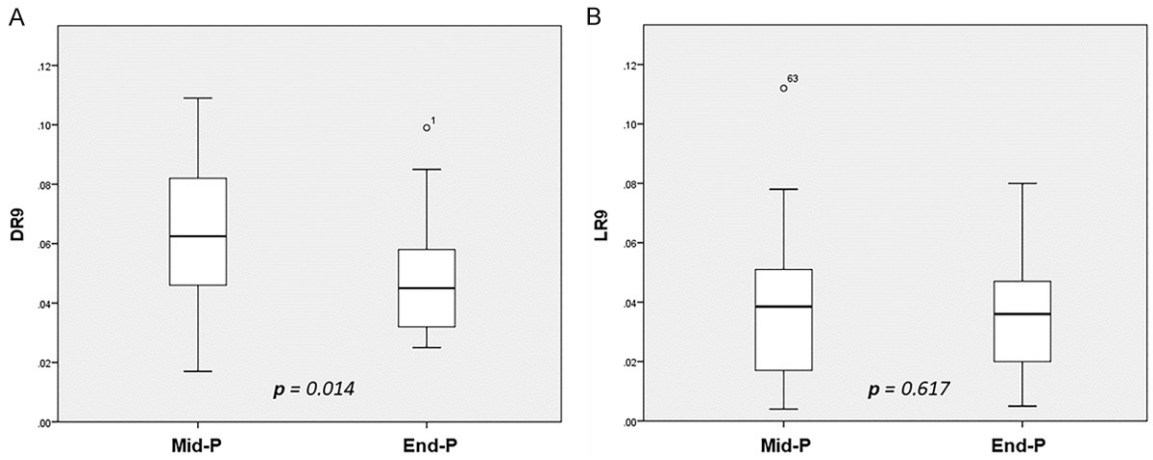

Figure 2. DR9 values in Mid-P and End-P groups (A). LR9 values in Mid-P and End-P groups (B). *P-values* are shown in the graphs. Abbreviations: Mid-P (Mid-Pregnancy), End-P (End-Pregnancy), DR9 (Dark Ratio, when k = 9 in k-means algorithm), LR9 (Light Ratio, when k = 9 in k-means algorithm).

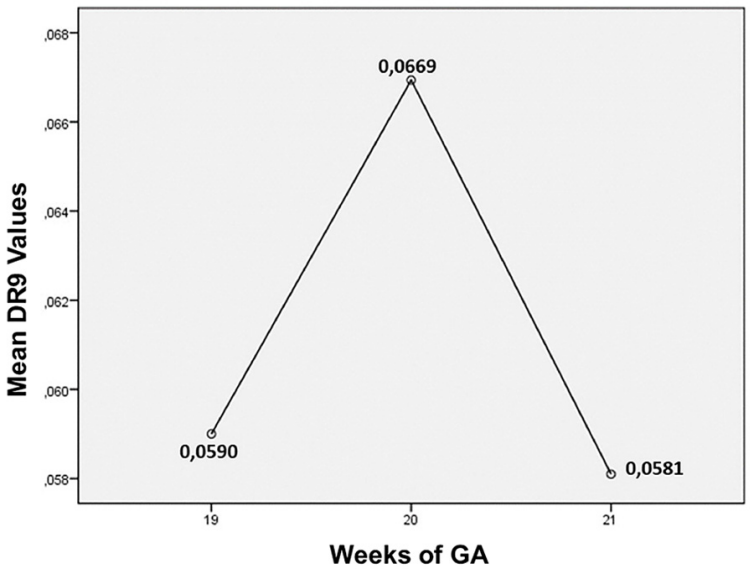

Figure 3. Mean DR9 values in Mid-P group at 19-21 weeks of GA. Abbreviations: Mid-P (Mid-Pregnancy), GA (Gestational Age), DR9 (Dark Ratio, when k = 9 in k-means algorithm).

t-test (parametric) and Mann-Whitney test (non-parametric) to investigate the differences of *DR9* in these two groups. All tests were performed by using IBM SPSS® Statistics 21.0 and only $p < 0.05$ results were considered statistically significant.

Results

Shapiro-Wilk normality test showed a normal distribution of variables except for a non-normal distribution of *DR9* in the End-P group. Pearson rank test showed a significant correlation between *DR9* and weeks of gestation (r = -0.298, *p*-value = 0.021). Height, weight, body mass index and age of the patients did not correlate to the DR9 or LR9. Results from Pearson correlation test are shown in **Table 3**. Independent samples t-test showed a difference between the *DR9* in Mid-P versus End-P (0.0631 and 0.0483 respectively - $p = 0.014$). Because of the non-normal distribution of *DR9* in End-P group, we performed Mann-Whitney test, which showed comparable results ($p = 0.023$). *LR9* did not show any difference between groups: $p = 0.617$ (**Figure 2**).

Discussion and conclusion

Previous applications of US in foetal spleen evaluation were merely focused on morphological description (shape, dimensions) [20, 31, 32] or in assessing parenchymal lesions [33]. Currently, no data are available on US-definition of normal/healthy foetal spleen parenchyma: its echogenicity was simply defined as similar to that of liver and kidneys [21]. This study represents the first US-based assessment of healthy spleen parenchyma in two GAs (Mid-P vs End-P), during which this organ seems to play different roles (haematopoietic vs non-haematopoietic) [3, 4, 6]. The variation

of splenic echogenicity is hard to appreciate without an image processing computer system, which generates radiomic parameters related to echogenicity (DR and LR). The application of radiomics to US technique and the expansion of this new challenging field to prenatal US screenings seems to be a rapidly expanding phenomenon [34-36].

Our results show that sonographic appearance of spleen may change during the course of pregnancy. This may reflect a different activity of spleen between the fifth and ninth month. The difference is significant in *DR9* ($p = 0.021$): we speculate that the difference in anechoic/dark signals during these GAs may depend on different cell populations, rather than vascular structure. The slight difference between the two groups is non-significant ($p = 0.617$) in *LR9*: this may hypothetically reflect a similar architecture of hyperechoic regions.

In fact, considering the equivalent vascular development of foetal spleen at 22nd and 38th GA [11], we believe that darker sonographic signal in Mid-P group correlates with higher density of HSCs and this may impact on the echogenicity of spleen parenchyma.

HSCs can be collected from the spleen during 13th to 36th weeks of GA [11], but these are undetected at ninth month, when splenic haematopoiesis is described to stop [6]. This finding could support the hypothesis that spleen may contribute as a minor and transient haematopoietic organ in foetal life.

Interestingly, based on DR values progression (**Figure 3**) in Mid-P group, the spleen exhibits its darker appearance at the 20th week of GA. This event could represent the peak of splenic HSCs due to a greater haematopoietic or trapping activity [9]. The difference between *DR9* mean at 20th week of GA versus End-P group was statistically significant ($P = 0.008$).

This study represents the first attempt to examine an historical controversy using US, a non-invasive and widespread technique. Considering that histology of spleen cannot be investigated in living foetuses, US-based radiomic analysis could represent a valid approach to evaluate splenic structure and activity. Ideally, the sonographic appearance of spleen should be followed throughout the whole gestation and in a larger cohort of pregnant women.

We also believe this novel strategy could be employed as modern imaging approach to explore EMH in adult pathological conditions, such as myeloproliferative neoplasms. The characterization of this phenomenon could be the first step for a future non-invasive diagnostic tool and provide useful information regarding prognosis and response-to-treatment of these conditions.

Disclosure of conflict of interest

None.

Address correspondence to: Dr. Vincenzo Martinelli, Department of Medicine and Health Sciences "Vincenzo Tiberio", University of Molise, Campobasso, Italy; C/da Tappino, 86100 Campobasso, CB, Italy; Haematology Department, Federico II University, Via S. Pasini, 5, 80131 Naples, NA, Italy. E-mail: vincenzo.martinelli@unimol.it

References

[1] Mebius RE and Kraal G. Structure and function of the spleen. Nat Rev Immunol 2005; 5: 606-616.

[2] Mukhia R, Mukherjee A and Sabnis A. Histogenesis of human fetal spleen. Int J Anat Res 2016; 4: 2119-2124.

[3] Dor FJ, Ramirez ML, Parmar K, Altman EL, Huang CA, Down JD and Cooper DK. Primitive hematopoietic cell populations reside in the spleen: studies in the pig, baboon, and human. Exp Hematol 2006; 34: 1573-1582.

[4] Crosby WH. Hematopoiesis in the human spleen. Arch Intern Med 1983; 143: 1321-1322.

[5] Forestier F, Daffos F, Catherine N, Renard M and Andreux JP. Developmental hematopoiesis in normal human fetal blood. Blood 1991; 77: 2360-2363.

[6] Varga I, Galfiova P, Adamkov M, Danisovic L, Polak S, Kubikova E and Galbavy S. Congenital anomalies of the spleen from an embryological point of view. Med Sci Monit 2009; 15: RA269-276.

[7] Freedman MH and Saunders EF. Hematopoiesis in the human spleen. Am J Hematol 1981; 11: 271-275.

[8] Sharma S, Pati HP, Ahuja RK, Takkar D and Kochupillai V. Haemopoietic cell composition of human fetal liver, spleen and thymus. Med Oncol 1997; 14: 99-101.

[9] Calhoun DA, Li Y, Braylan RC and Christensen RD. Assessment of the contribution of the spleen to granulocytopoiesis and erythropoiesis of the mid-gestation human fetus. Early Hum Dev 1996; 46: 217-27.

[10] Hann IM, Bodger MP and Hoffbrand AV. Development of pluripotent hematopoietic progenitor cells in the human fetus. Blood 1983; 62: 118-123.
[11] Holkunde A and Sakhare S. The histological study of human fetal spleen. Indian J Clin Anat Physiol 2018; 5: 260-265.
[12] Djaldetti M. Hemopoietic events in human embryonic spleens at early gestational stages. Biol Neonate 1979; 36: 133-44.
[13] Wolf BC, Luevano E and Neiman RS. Evidence to suggest that the human fetal spleen is not a hematopoietic organ. Am J Clin Pathol 1983; 80: 140-4.
[14] Wilkins BS, Green A, Wild AE and Jones DB. Extramedullary haemopoiesis in fetal and adult human spleen: a quantitative immunohistological study. Histopathology 1994; 24: 241-247.
[15] Barker JN, Kempenich J, Kurtzberg J, Brunstein CG, Delaney C, Milano F, Politikos I, Shpall EJ, Scaradavou A and Dehn J. CD34(+) cell content of 126 341 cord blood units in the US inventory: implications for transplantation and banking. Blood Adv 2019; 3: 1267-1271.
[16] Wilpshaar J, Joekes EC, Lim FT, Van Leeuwen GA, Van den Boogaard PJ, Kanhai HH, Willemze R and Falkenburg JH. Magnetic resonance imaging of fetal bone marrow for quantitative definition of the human fetal stem cell compartment. Blood 2002; 100: 451-457.
[17] Chiu SC, Liu HH, Chen CL, Chen PR, Liu MC, Lin SZ and Chang KT. Extramedullary hematopoiesis (EMH) in laboratory animals: offering an insight into stem cell research. Cell Transplant 2015; 24: 349-66.
[18] Kim CH. Homeostatic and pathogenic extramedullary hematopoiesis. J Blood Med 2010; 1: 13-19.
[19] Yamamoto K, Miwa Y, Abe-Suzuki S, Abe S, Kirimura S, Onishi I, Kitagawa M and Kurata M. Extramedullary hematopoiesis: elucidating the function of the hematopoietic stem cell niche (Review). Mol Med Rep 2016; 13: 587-591.
[20] Aoki S, Hata T and Kitao M. Ultrasonographic assessment of fetal and neonatal spleen. Am J Perinatol 1992; 9: 361-367.
[21] Schmidt W, Yarkoni S, Jeanty P, Grannum P and Hobbins JC. Sonographic measurements of the fetal spleen: clinical implications. J Ultrasound Med 1985; 4: 667-672.
[22] Edwards L and Hui L. First and second trimester screening for fetal structural anomalies. Semin Fetal Neonatal Med 2018; 23: 102-111.
[23] Torrents-Barrena J, Monill N, Piella G, Gratacos E, Eixarch E, Ceresa M and Gonzalez Ballester MA. Assessment of radiomics and deep learning for the segmentation of fetal and maternal anatomy in magnetic resonance imaging and ultrasound. Acad Radiol 2021; 28: 173-188.
[24] Wang X, Sun J, Zhang W, Yang X, Zhu C, Pan B, Zeng Y, Xu J, Chen X and Shen X. Use of radiomics to extract splenic features to predict prognosis of patients with gastric cancer. Eur J Surg Oncol 2020; 46: 1932-1940.
[25] Avanzo M, Stancanello J and El Naqa I. Beyond imaging: the promise of radiomics. Phys Med 2017; 38: 122-139.
[26] Yuan C and Yang H. Research on k-value selection method of k-means clustering algorithm. Multidisciplinary Scientific Journal 2019.
[27] You JH, Lv GR, Liu XL and He SZ. Reference ranges of fetal spleen biometric parameters and volume assessed by three-dimensional ultrasound and their applicability in spleen malformations. Prenat Diagn 2014; 34: 1189-1197.
[28] Lambin P, Leijenaar RTH, Deist TM, Peerlings J, de Jong EEC, van Timmeren J, Sanduleanu S, Larue RTHM, Even AJG, Jochems A, van Wijk Y, Woodruff H, van Soest J, Lustberg T, Roelofs E, van Elmpt W, Dekker A, Mottaghy FM, Wildberger JE and Walsh S. Radiomics: the bridge between medical imaging and personalized medicine. Nat Rev Clin Oncol 2017; 14: 749-762.
[29] David A and Vassilvitskii S. K-Means++: the advantages of careful seeding. Symp on Discrete Algorithms 2007; 8: 1027-1035.
[30] Yap BW and Sim CH. Comparisons of various types of normality tests. J Stat Comput Simul 2011; 81: 2141-2155.
[31] Moreira M, Bras R, Goncalves D, Alencoao I, Inocencio G, Rodrigues M and Braga J. Fetal splenomegaly: a review. Ultrasound Q 2018; 34: 32-33.
[32] Chaoui R, Zodan-Marin T and Wisser J. Marked splenomegaly in fetal cytomegalovirus infection: detection supported by three-dimensional power Doppler ultrasound. Ultrasound Obstet Gynecol 2002; 20: 299-302.
[33] Sepulveda W, Ochoa JH, Cafici D, Wong AE, Badano F, Andreeva E and Andreeva EY. Splenic cyst as a rare cause of fetal abdominal cystic mass: a multicenter series of nine cases and review of the literature. Ultrasound 2018; 26: 22-31.
[34] Sun Y, Zhang L, Dong D, Li X, Wang J, Yin C, Poon LC, Tian J and Wu Q. First-trimester screening for trisomy 21 via an individualized nomogram. Ultrasound Obstet Gynecol 2020; [Epub ahead of print].

[35] Du Y, Fang Z, Jiao BDJ, Xi G, Zhu C, Ren Y, Guo Y and Wang Y. Application of ultrasound-based radiomics technology in fetal lung texture analysis in pregnancies complicated by gestational diabetes or pre-eclampsia. Ultrasound Obstet Gynecol 2020; [Epub ahead of print].

[36] Dong Y, Zhou L, Xia W, Zhao XY, Zhang Q, Jian JM, Gao X and Wang WP. Preoperative prediction of microvascular invasion in hepatocellular carcinoma: initial application of a radiomic algorithm based on grayscale ultrasound images. Front Oncol 2020; 10: 353.